A Circularly Polarized Quad-band Annular Ring Antenna with Asymmetric Ground Plane Using Theory of Characteristic Modes

Reshmi Dhara[1, *], Sanjeev Yadav[2], Mahendra M. Sharma[3], Sanjay K. Jana[1], and Mahesh C. Govil[1, 3]

Abstract—Herein a theory of characteristic mode (TCM)-based design of circularly-polarized (CP) quad-band compact microstrip antenna is proposed. It involves one annular ring radiator having eight symmetrical slots along its boundary and three circular closed ring resonators (CRRs) on the bottom side of the substrate. Initially, CM analysis was carried out for the radiator without a feeding structure, to determine the modal currents and their corresponding modal fields (radiation patterns) of existing modes. This helped in recognizing the symmetric modes to be selectively excited by the feed to furnish CP and gave direction for selecting an asymmetric CPW-fed structure as the feed of choice. Evolution process of the antenna geometry shows that the eight symmetrical slots in tandem with the CRRs generate wide impedance bandwidth (IBW), while measured quad CP bands are obtained through uses of an asymmetric ground plane resonating at 5.63 GHz (120 MHz), a cross-shaped slit at 7.69 GHz (650 MHz), a rectangular open loop at 9.91 GHz (1200 MHz), and a tuning stub in the feeding structure at 12.09 GHz (160 MHz). Series of parasitic strips augmented CP radiation and eliminate ripples in the radiation pattern. Measured findings relate satisfactorily with simulations done using Ansys HFSS 2020 R1. A low cost FR-4 substrate is used to fabricate the antenna with an optimized dimension of $35 \times 30 \times 1.6\,\text{mm}^3$. The measured IBW ranges from 4.36–4.82 GHz, 5.50–5.78 GHz, and 5.95–beyond 14 GHz. The proposed antenna may find suitable applications in C band, X band, and 5 GHz WLAN devices.

1. INTRODUCTION

In contemporary wireless communication devices, there is an enduring challenge for developing miniaturized, multiband, and cost-effective antennas. Circular polarization technique has become an attractive choice due to its high immunity against multipath interferences, heftiness to polarization mismatches, and reliable transmission characteristics in hostile weather conditions [1]. Circular polarization can be generated using either double or single feed mechanism in microstrip antennas. Dual feeds generate broad CP bands, but they require external power dividers and extra space, which becomes problematic for fabricating compact microstip antennas [2]. Therefore, single feed mechanism for generating CP radiation is more desirable in terms of easy fabrication. In single feed mechanism, principal scheme involves detuning of the degenerate mode in a symmetrical patch by implementing minor modifications in geometry at suitable positions to perturb electric fields. The generated mode of a patch antenna can be divided into two orthogonal modes by well-studied perturbation sections like slits, slots, truncated segments, or stubs [3]. The radiation fields excited by these modes are typically perpendicular to each other. These two modes can be tuned to equal amplitude and phase quadrature at the resonant frequency by optimizing the amount of perturbation created. In this way, CP radiation with

* Corresponding author: Reshmi Dhara (reshmidhara@nitsikkim.ac.in).
[1] National Institute of Technology Sikkim, Ravangla 737139, India. [2] Government Women Engineering College Ajmer, Ajmer, Rajasthan 305002, India. [3] Malviya National Institute of Technology, Jaipur 302017, India.

considerably enhanced bandwidth can be attained employing single feed. Nowadays, multiple circularly polarized antennas are replaced by a single antenna which satisfies multiple band operation. Slot antenna [4–8] research has greatly impacted various fields like telecommunication, medical, military, and commercial applications by helping in realizing miniaturized microstrip antennas needed in these areas. Very recently, a triple band circularly polarized antenna has been demonstrated using slot/strips [9]. Optimization of slot antennas by utilizing single feed mechanism to achieve circularly polarized quad bands remains a challenging area which needs urgent attention of researchers. Recently, some antennas have been developed using single feed to achieve either quad- or multi bands [10–13].

The theory of characteristic modes (TCM) was proposed way back in 1971 by Garbacz and Turpin [14], and later improvised by Harrington and Mautz [15, 16]. Recently, a resurrection of interest in TCM is observed for designing microstrip antennas. It provides a plain understanding of every resonant mode, the equivalent mode current, and its far field radiation pattern. These details can also give significant control during designing best feeding network and desired polarization properties [17]. TCM analysis is also a good tool for antenna placement studies for platforms that are inherently part of the radiator. In recent times, TCM has been applied in designing many wideband antennas [18–24]. However, many of these antennas lacked stable radiation patterns while trying to achieve wide IBW. Very recently, we have also used TCM to design a circularly polarized coplanar waveguide (CPW)-fed slot antenna [25]. The antenna is designed using theoretical lower resonating frequency 4.38 GHz so that it can cover some channel of 802.11 standards used for Wi-Fi communications. Moreover, in many countries like India, bands in this frequency region have been kept unlicensed and free usage allowed for Wi-Fi and 5G communications. This motivated us to design a microstrip antenna envisaging 4.38 GHz as the theoretical lower resonating frequency.

Herein using TCM, a wide impedance and circularly polarized bands antenna simultaneously showing stable omnidirectional radiation patterns is proposed. It has been realized using eight symmetrical slots on the edge of an annular radiator as it can generate wide impedance band compared to a conventional rectangular microstrip antenna. Initially, CM analysis of the radiator, without feeding, was carried out to identify the existing desired symmetric modes. A modified asymmetric CPW-fed ground is chosen as the preferred feeding network to excite the identified desired modes without excitation of undesired anti-symmetric modes. Three CRRs on the opposite side of the substrate are used for increasing coupling with the radiator to provide widened IBW. A series of parasitic strips along the edge of the annular radiator enhanced CP radiation and eliminated ripples in the radiation pattern. The asymmetric cross-shaped slit at the centre of the annular radiator provides CP radiation at 7.69 GHz. The coupling effect between the annular ring radiator and a smaller open loop resonator placed near the right corner of this main radiator played a pivotal role in obtaining circular polarization band at 9.91 GHz. The tuning stub on the feed furnished another CP band at 12.09 GHz and further widened the overall IBW. Asymmetric CPW-fed technique has been used for feeding to excite the desired symmetric modes and create optimized perturbations required to obtain another CP band at 5.63 GHz. The measured quad CP bands are well inside the ranges of measured and simulated IBWs. Simulations were carried out using *Ansys HFSS 2020 R1* based on the Finite Element Method (FEM). The achieved very wide CP bands of the antenna can be used for various applications in C, X and Ku bands.

The paper is organized as follows, Section 2: Antenna Configuration; Section 3: TCM Analysis; Section 4: Choosing Appropriate Feeding for Excitation of Identified Useful Modes; Section 5: Experimental Validations and Discussions; and Section 6: Conclusion.

2. ANTENNA CONFIGURATION

To elaborate the design evolution process, five antenna structures are defined in Figs. 1(a)–(e). Simulated IBW and axial ratio bandwidth (ARBW) curves of these five antenna designs are presented in Figs. 2(a) and (b), respectively. In Antenna.1, eight symmetrical slots are etched around the edge of the annular radiator [26] to obtain wide impedance band at upper frequency boundary, and on the edge of the radiating element an array of parasitic strips are utilized to achieve CP radiation. Antenna.1 gave two small impedance bands, and ARBW values were too large (> 3 dB). In the next step to improve antenna performance, use of an asymmetrical cross shaped slit [2] with optimized long arm and short
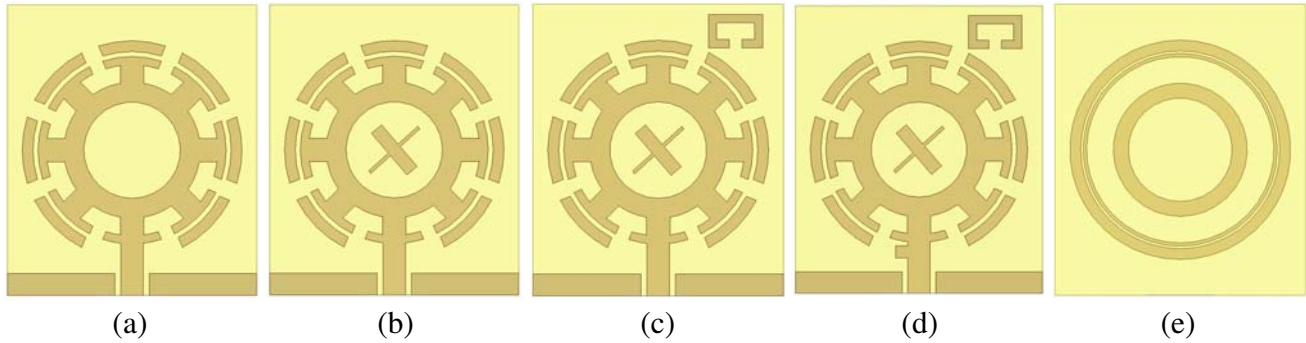
Figure 1. Five improvement stages for design of antenna: (a) Antenna.1 top view, (b) Antenna.2 top view, (c) Antenna.3 top view, (d) Antenna.4 and Antenna.5 top view, (e) Antenna.5 bottom view.
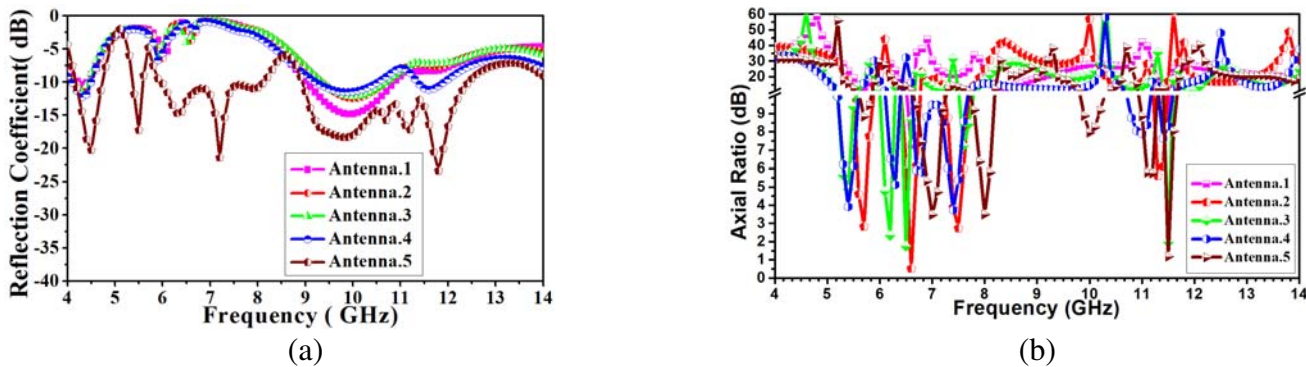

Figure 2. Improvement for five stages of design of antenna: (a) Reflection coefficient and (b) axial ratio bandwidth.

arm and cross angles $42.5°$ and $130.5°$, respectively, helped in obtaining circular polarization in the middle range of frequency for Antenna.2. In next step, near the right most corner of the radiating element, a rectangular open loop is placed to create the coupling effect between the radiator and open loop, which further improved circular polarization in the middle frequency range for Antenna.3 [27]. A tuning stub added on the feeding element [28] in Antenna.4 helped in achieving a CP band at the upper range of frequency and widen IBW as well. Antenna.5 was designed, to obtain wide IBW at upper frequency range, by employing three circular CRRs [29] on the bottom side of the substrate. This resulted in significant increase in IBW as well as furnished four wide IBWs. Two are in lower frequency range (4.15–4.75 GHz, 5.4–5.55 GHz) and the other two at higher frequency range (5.95–8.12 GHz, 8.95–12.45 GHz).

The configuration and dimensions of the radiator without feed are presented in Fig. 3.

Optimized Dimensions for radiator without feed (all in mm): $Ls = 35$, $Ws = 30$, $h = 1.6$, $r1 = 5.8$, $r2 = 11.3$, $r3 = 10.3$, $r4 = 13.2$, $r5 = 11.9$, $r6 = 8.2$, $L3 = 6.6$, $L4 = 8$, $L5 = 1.5$, $L6 = 4$, $S1 = 0.7$, $S2 = 0.6$, $S3 = 1.7$, $S4 = 2.8$, $S5 = 2.2$, $Lf = 6.28$, $W3 = 1.6$, $W4 = 0.4$, $W5 = 1.5$, $Wf = 2.7$, $c1 = 6.5$, $c2 = 4.5$, $c3 = 1.5$, $d = 1$, $\phi1 = 42.5°$, $\phi2 = 130.5°$.

3. THEORY OF CHARACTERISTICS MODE ANALYSIS

At the fundamental mode, the current flows on the whole antenna, contributing to radiation at lower frequencies. On the other hand, at higher modes, the mode current mainly flows on the edge of the radiator contributing to radiation at higher frequencies. That presents flexibility to modify the phase of the far zone electric field as additional radiating modes are concerned.

With the aim to broaden impedance and circularly polarized bandwidth of an antenna, it is desired
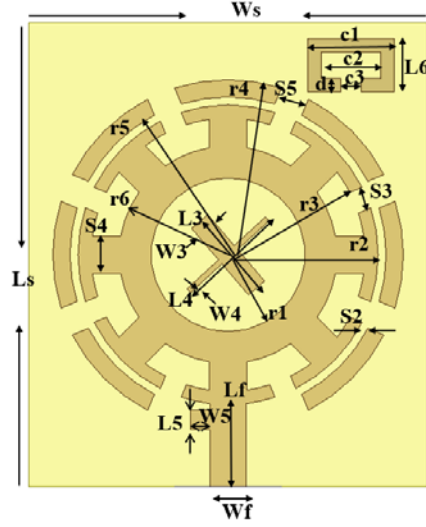
Figure 3. Top view of proposed antenna without feeding and ground plane.

to know the existing modes in the radiator. To realize the potential of the modified annular ring antenna providing wide operating frequency bands, it was needed to know the existing modes within it. So, TCM analysis was carried out to identify the desired modes to be excited in x and y directions. For the ease of understanding, some equations of TCM are briefly discussed below. More details about TCM analyses are available in [14–24].

3.1. Theory of Characteristic Modes

Provided a typical conducting element, any electric current $(\vec{J})$ on its surface is defined as a total of characteristic modes or eigen currents $(\overrightarrow{J_n})$ with different product coefficients (α_n):

$$\vec{J} = \sum_n \alpha_n \overrightarrow{J_n} = \sum_n \frac{V_n^i \overrightarrow{J_n}}{1 + j\lambda_n} \tag{1}$$

where $\overrightarrow{J_n}$ are the eigen currents; λ_n are the eigen values; α_n are the modal weighting coefficients; and V_n^i are the modal excitation coefficients, which are expressed by:

$$V_n^i = \left\langle \overrightarrow{J_n}, \overrightarrow{E^i} \right\rangle = \oiint_{s=0}^{s} \overrightarrow{J_n} \cdot \overrightarrow{E^i} ds \tag{2}$$

where $\overrightarrow{E^i}$ is the impressed source. Modal weighting coefficient α_n can be obtained by means of the following equation:

$$\alpha_n = \frac{V_n^i}{1 + j\lambda_n} \tag{3}$$

Modal significance (MS_n) is generally used to estimate the radiation efficiency of a mode. Then MS_n can be calculated as:

$$MS_n = \left| \frac{1}{1 + j\lambda_n} \right| \tag{4}$$

One more significant parameter that is exploited for the design of the antenna is characteristic angle β_n, which can be expressed as:

$$\beta_n = 180° - \tan^{-1}(\lambda_n) \tag{5}$$

In the case of a resonant mode, $\overrightarrow{J_n}$ viz. $\lambda_n = 0$, $MS_n = 1$, and $\beta_n = 180°$ from Eqs. (4) and (5), respectively. When a mode is excited, it radiates maximum energy when $\beta_n = 180°$, and the closer the

β_n approaches 180° or λ_n towards 0, the more efficiently the mode radiates. As per expression (1), how efficiently a mode $\overrightarrow{J_n}$ is excited relies on the modal weighting of α_n coefficient. For the time being, α_n is regulated by two parameters, i.e., λ_n eigenvalues and modal excitation coefficients V_n^i. When a mode is resonating at its resonance frequency, λ_n equals 0. Therefore, Equation (3) may be modified as:

$$\alpha_n = V_n^i \tag{6}$$

In the case of some non-resonant modes, their eigenvalues are quite large over the observed frequency band. This implies that irrespective of a conducting object or the antenna is excited, the modal weighting coefficient is generally quite small. These modes are commonly considered as unimportant modes. For a more relevant and simpler study, significant modes are considered, whose characteristic angles are near 180°. Using formula (3), when eigenvalue λ_n is static, the modal weighting coefficient is completely controlled by how the antenna is excited. Following Eq. (2), in order to get a comparatively high value of modal weighting coefficient, the excitation must be placed where the eigen current is quite high.

So Equation (3) is the condition to obtain the desired mode, and preciously a large modal significance is needed, but also a large modal excitation coefficient V_n is required. The modal excitation depends on the properties of feeding such as the feeding type, feeding position, and feeding dimensions. In the following subsection, the modes of the proposed antenna are analyzed in detail.

3.2. Identification of the Existing Symmetric Modes to Be Excited

In this section, the antenna without feeding structure is analyzed using TCM. To make the process simpler, an ideal environment is envisioned, where the antenna is assumed to be a perfect conductor with zero thickness and without any substrate. The Characteristic Mode Analysis Solver is the IE analogue to the FEM eigen solver. All the characteristics mode simulations were carried out using Ansys Electronics Desktop 2020 R1 and presented in Fig. 4.
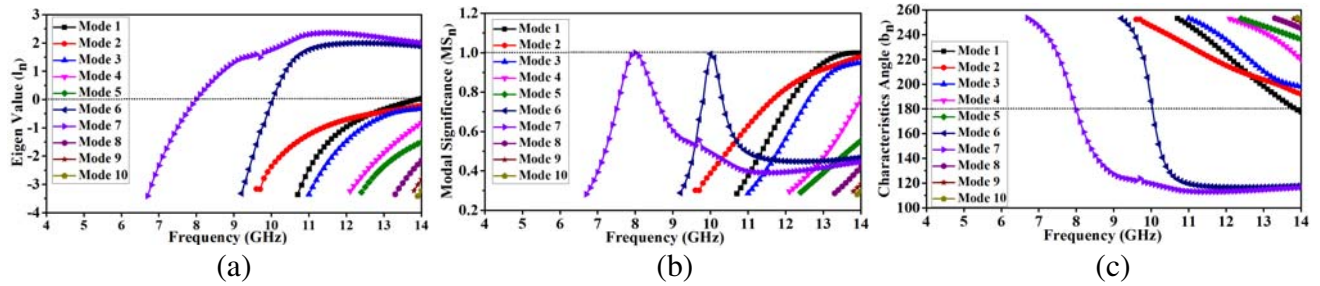

Figure 4. Characteristics mode analysis: (a) Eigen value (λ_n), (b) modal significance (MS_n) and (c) characteristics angle (β_n).

From Fig. 4(a) it is found for the modified annular ring radiator that there are total ten modes out of which three modes' eigenvalues (λ_n) approach zero. Here, $\lambda_n > 0$ indicative of a mode that stores electrical energy, whereas $\lambda_n < 0$ indicates a mode that stores magnetic energy, and $\lambda_n = 0$ indicative of a mode that is resonant and easily excited by plane wave.

For the radiator, there are no dominant modes observed lower than 7.99 GHz and more than 13.86 GHz as clearly seen from Modal Significance curves in Fig. 4(b). As the eigenvalue goes to zero, it resonates; the Modal Significance goes to 1 for three modes (Modes 1, 6, and 7 dominant frequency 13.86 GHz, 10.03 GHz and 7.99 GHz).

Figure 4(c) shows the characteristic angle β_n curves where the same three resonant modes appeared as $\beta_n = 180°$. When β_n equals 90° or 270°, it only stores energy, but when it is around $\beta_n = 180°$, it radiates strongly.

This implies that to excite the radiating element at frequency lower than 7.99 GHz in order to obtain wide IBW using the same radiator with high efficiency and stable high gain, a suitable feeding technique with a proper ground plane and tuning or matching network will be required.
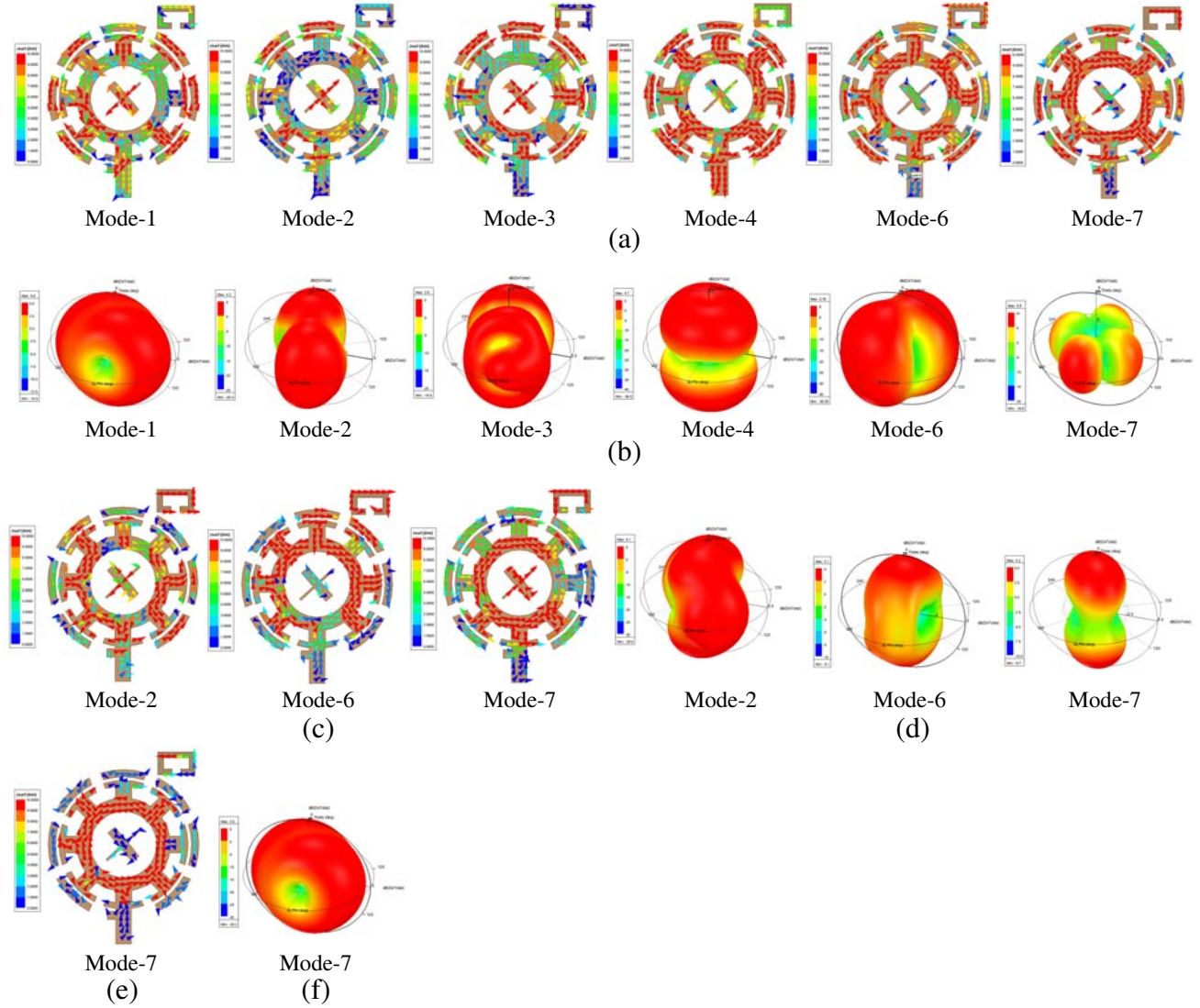
Mode-1   Mode-2   Mode-3   Mode-4   Mode-6   Mode-7
(a)

Mode-1   Mode-2   Mode-3   Mode-4   Mode-6   Mode-7
(b)

Mode-2   Mode-6   Mode-7   Mode-2   Mode-6   Mode-7
(c)   (d)

Mode-7   Mode-7
(e)   (f)

Figure 5. Modal currents (a), (c), (e) and radiation pattern (b), (d), (f) without feeding network of 10 modes (desired and undesired) at broadside direction. (a) Modal surface current distribution of 10 modes at 12.06 GHz. (b) Modal field (far field radiation pattern) of 10 modes at 12.06 GHz. (c) Modal surface current distribution of 10 modes at 9.91 GHz. (d) Modal field (far field radiation pattern) of 10 modes at 9.91 GHz. (e) Modal surface current distribution of 10 modes at 7.69 GHz. (f) Modal field (far field radiation pattern) of 10 modes at 12.06 GHz.

At higher frequency, more modes with relatively large modal significance are involved. In order to analyze [30–32] the modes of the antenna clearly, the current and far field of different characteristic modes were studied. Figs. 5(a)–(f) show the modal current distribution of the radiator for three desired existing modes at their CP resonating frequencies. Figs. 5(a)–(b) show that modes 1 and 6 are the fundamental modes in y and x directions, respectively, radiate in $+z$ direction at $f_{c4} = 12.09$ GHz, and constitute good main lobe. A circular polarization is produced due to these two modes as phase difference between them is $90°$. Modes 2, 3, 4, 7 lead to the cancelation of electric field in the far field zone at $+z$ direction and split the main lobe.

Figs. 5(c)–(d) show that modes 6 and 7 are the fundamental modes in x and y directions correspondingly and radiate in $+z$ direction at $f_{c3} = 9.91$ GHz. Again a circular polarization is produced as phase differences between them is $90°$. Mode 2 leads to the cancelation of electric field in the far

field zone at $+z$ direction and split the main lobe.

Figs. 5(e)–(f) show that mode 7 is the fundamental mode in y direction and radiates in $+z$ direction at $f_{c2} = 7.61\,\text{GHz}$. To generate circular polarization, a proper feeding technique is required in order to create another x directed mode orthogonal to mode 7.

So, after this characteristics mode analysis (CMA) analysis, a suitable feeding technique was searched in order to excite these desired existing dominant modes in the radiator. According to TCM extension, unacceptable modes (2, 3, 4, 5, 8, 9, and 10) might also get excited by feeding and then affect the total radiation pattern. Therefore, they should be moved out of the operating band or optimized with good patterns.

4. CHOOSING APPROPRIATE FEEDING FOR EXCITATION OF IDENTIFIED USEFUL MODES

From the above TCM analysis three desired modes (1, 6, and 7) were identified out of ten. It was further concluded that other seven modes (*viz.* 2, 3, 4, 5, 8, 9, and 10) were undesired modes and not useful. To achieve high gain at bore sight direction, a proper feeding method should provide a good impedance matching for the symmetric desired modes without the excitation of undesired anti-symmetric modes. Generally, only one mode has high modal significance value, and feeding techniques like microstrip-line feed, probe feed, aperture coupled feed, proximity coupled feed are used to feed a rectangular microstrip antenna (RMSA). However, the presence of multiple modes with high modal significance puts limitations to designing an appropriate feed. In those cases, CPW-fed is a preferred choice as it exerts least disturbance over a wide impedance band. To achieve circular polarization, it is necessary to create two orthogonal electric fields with equal amplitude and quadrature phase difference. This can be achieved if one can generate unequal current path lengths. So, asymmetric CPW-fed is one of the best choices to obtain CP at desired symmetric modes.

4.1. Selection of CPW-Fed and Its Effect on the Proposed Antenna

The CPW-fed is the feeding technique where side-plane conductor is the ground, and centre strip carries the signal. CPW-fed monopole antennas have been extensively investigated because of their many enticing features like wide IBW, light weight, and compact structure, and omnidirectional radiation characteristics. The CPW-fed can provide a large electric coupling between the radiator and the ground. CPW feeds [33] use a sole metallic layer basically generating trivial conjoint coupling among two fine-tune lines, to give wide bandwidth. They are quite common for their easy integration with solid state active devices or MMICs. When CPW-fed is asymmetric, because unequal path lengths generate wide band CP [34]. Accordingly, we intended to use asymmetric CPW-fed.

From Fig. 5, it is seen that the current and magnetic fields of mode 1, mode 6, and mode 7 are the highest along the edge of the radiator. Mode current distributions show that the magnetic current of the feed should be in the same direction of the mode current and be placed where the current is maximum. When the feed is positioned at centre, it will give the best symmetric current distribution with respect to xz or yz planes. These requirements can be best realized by employing a CPW-fed. Antenna.5 did not give wide IBW by using the modified annular ring radiator and a symmetric CPW-fed ground on the same plane of the substrate. However, TCM analysis indicated that using the same radiator, much wider IBW and ARBW can be obtained by exciting the desired dominant modes through another appropriate feeding structure, which in this case was found to be an asymmetric CPW-fed. This led to generation of three wide impedance bands (4.36–4.82 GHz, 5.50–5.78 GHz, 5.95–beyond 14 GHz), as well as three CP bands at desired dominant frequencies. Though modes 1, 6, 7 (13.86 GHz, 10.03 GHz and 7.99 GHz) exhibited slight shift (12.09 GHz, 10.03 GHz, and 7.69 GHz) after adding the asymmetric CPW-fed, the currents remained symmetric with respect to xz and yz planes, like the current of the modes without the CPW-fed. In addition, another CP mode was generated due to this feeding at $f_{c1} = 5.63\,\text{GHz}$, ranging 5.57–5.69 GHz. Thus, it becomes easy to achieve a wide impedance and CP bands by tuning the position, length, and width of the feed line. Design steps of the asymmetric CPW-fed are shown in Fig. 6, and their effect on the antenna performance is shown in Fig. 7.
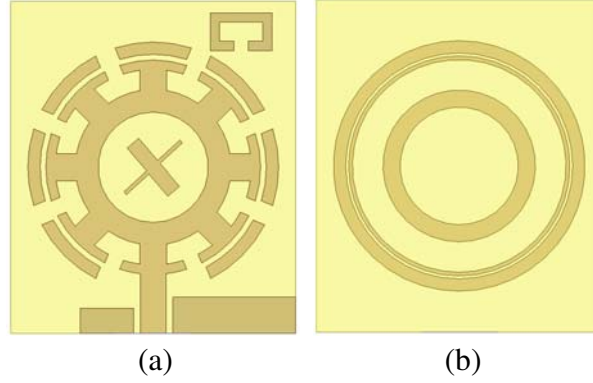
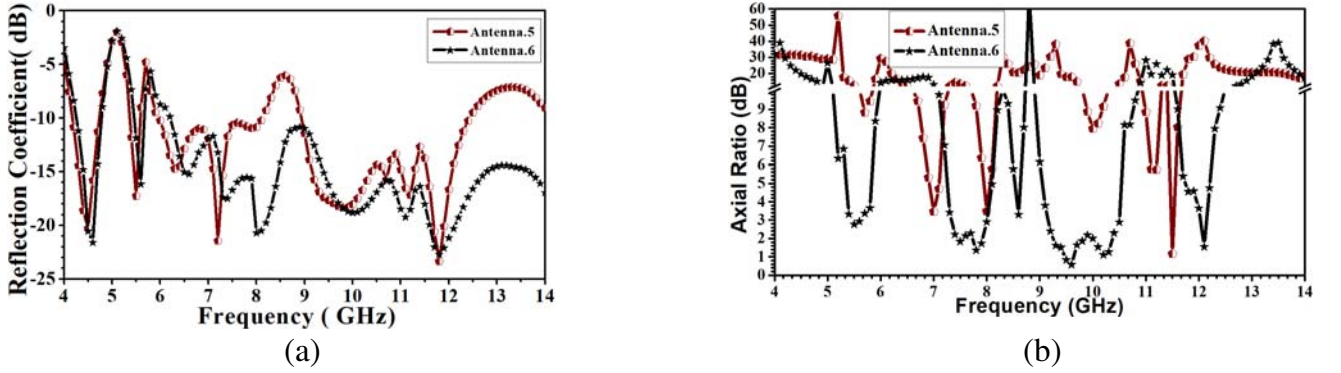**Figure 6.** Two improvement stages for design of antenna: (a) Antenna.6 top view, (b) Antenna.6 bottom view.

Figure 7. Improvement for two stages of design of antenna: (a) Reflection coefficient and (b) axial ratio bandwidth.

5. EXPERIMENTAL VALIDATIONS AND DISCUSSIONS

Figure 8 shows the simulated and fabricated monopole antennas. Figs. 8(a) and (b) depict the top and bottom views of simulated proposed antenna, whereas Figs. 8(c) and (d) represent them for the fabricated antenna. Dimension of the antenna is $35 \times 30\,\text{mm}^2$ ($0.84 \times 0.72\lambda_{gL}^2$, where λ_{gL} is the guided wavelength at measured lower resonating frequency 4.38 GHz). It was fabricated on an FR4-epoxy substrate (dielectric constant $\varepsilon_r = 4.4$, $\tan\delta = 0.02$). The optimized dimensions of the fabricated antenna are listed below.

Optimized Dimensions for Proposed Antenna (all in mm): $L1 = 3.8$, $L2 = 2.6$, $S1 = 0.7$, $W1 = 13$, $W2 = 5.65$, $R1 = 13.2$, $R2 = 11.9$, $R3 = 11.6$, $R4 = 11.2$, $R5 = 8$, $R6 = 6.2$.

5.1. Experimental Data

Ansys Electronics Desktop 2020 R1 was used for simulations. Agilent Technologies, PNA-L Network Analyzer-N5234A (10 MHz–43.5 GHz) VNA, were used to perform the IBW measurement. Fig. 9(a) shows the comparison between measured and simulated return losses of the implemented antenna up to 14 GHz. The measured IBWs are 4.36–4.82 GHz, 5.50–5.78 GHz, and 5.95–beyond 14 GHz. The corresponding simulated 10-dB IBWs are 4.26–4.78 GHz, 5.46–5.67 GHz, and 6.21–beyond 14 GHz.

Figure 9(b) shows the comparison between measured and simulated ARBW curves. Measured curve spans 120 MHz (5.57–5.69 GHz, $f_{cp1} = 5.63$ GHz), 650 MHz (7.36–8.01 GHz, $f_{cp2} = 7.69$ GHz), 1200 MHz (9.31–10.51 GHz, $f_{cp3} = 9.91$ GHz), and 160 MHz (12.01–12.17 GHz, $f_{cp4} = 12.09$ GHz), whereas simulated curves span 180 MHz (5.42–5.53 GHz and 5.61–5.68 GHz), 700 MHz (7.32–8.02 GHz),
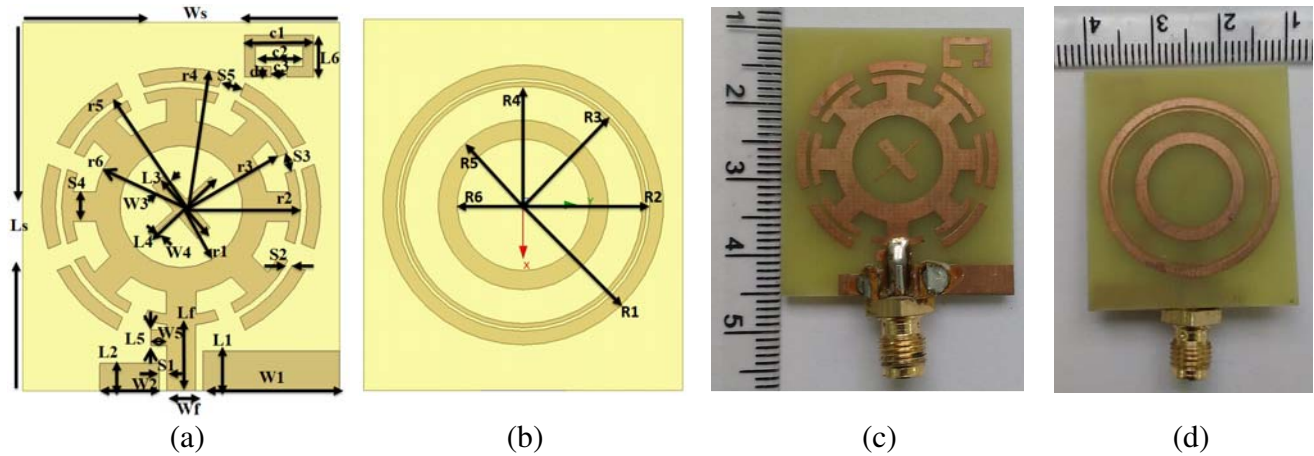
Figure 8. Dimensions of antenna simulated and fabricated. (a) Top view, (b) bottom view and (c) top view, (d) bottom view.
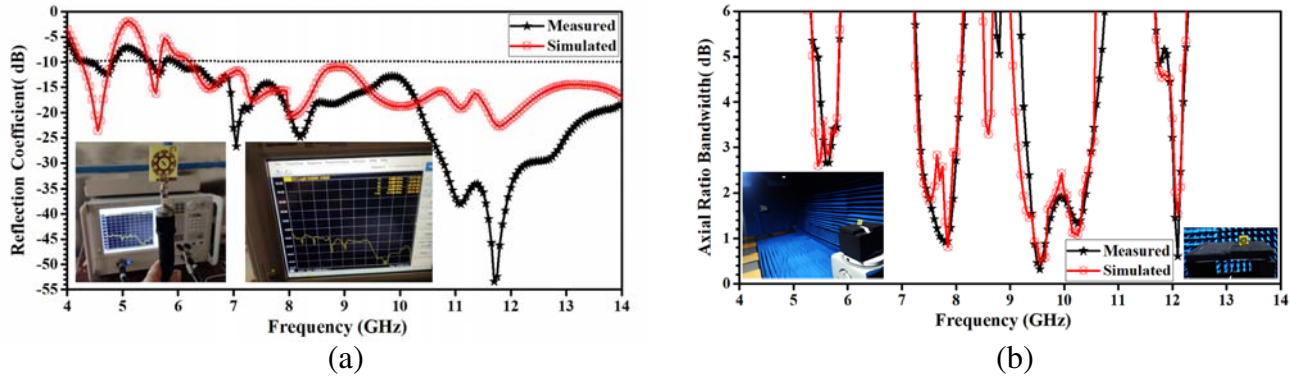

Figure 9. Comparison of measured and simulated. (a) Reflection coefficient curves and (b) ARBW curves.

1390 MHz (9.15–10.54 GHz), and 170 MHz (12.02–12.19 GHz, $f_{cp4} = 12.09$ GHz). All four CP bands are within the range of measured and simulated IBWs. Therefore, the proposed antenna can well be used for some C-band and ITU (8 GHz) applications. The first measured CP band can be used for 5 GHz WLAN 5570–5650 MHz band application. The second CP band can be used for FIXED Satellite communication. The third CP band may find use in Earth exploration satellite communication and radio location application, and lastly the fourth CP band may be used for FIXED Satellite (Space to Earth) communication.

Well defined, measured left hand circular polarization (LHCP) and right hand circular polarization (RHCP) are observed in Figs. 10(a), (c), (e), (g) and (b), (d), (f), (h) which depict the radiation patterns at $\varphi = 0°$ (XZ plane) and $\varphi = 90°$ (YZ plane) at $f_{c1} = 5.63$ GHz, $f_{c2} = 7.69$ GHz, $f_{c3} = 9.91$ GHz, $f_{c4} = 12.09$ GHz. It is found at CP resonating frequencies on the broadside direction that the radiations are LHCP, LHCP, RHCP, and LHCP, while the measured co-polarizations are greater than cross-polarization levels by 17 dBi, 25 dBi, 19 dBi, 29 dBi, respectively.

Figure 11(a) depicts the measured and simulated radiation efficiencies for the implemented antenna with respect to frequency. The simulated and measured radiation efficiencies are in the range of 63%–92% for all CP bands, and the measured efficiency is maximum at 6.52 GHz, 92%. Fig. 11(a) also shows the measured and simulated peak gains. The maximum measured peak gain is 5.38 dBi at 10.2 GHz.

Figure 11(b) shows that the magnitude of E_x/E_y is nearly equal to 1 or 0 dB over the range of quad CP bands, and the phase difference between them is also around 90°. This proves that the quad bands satisfy CP criteria.
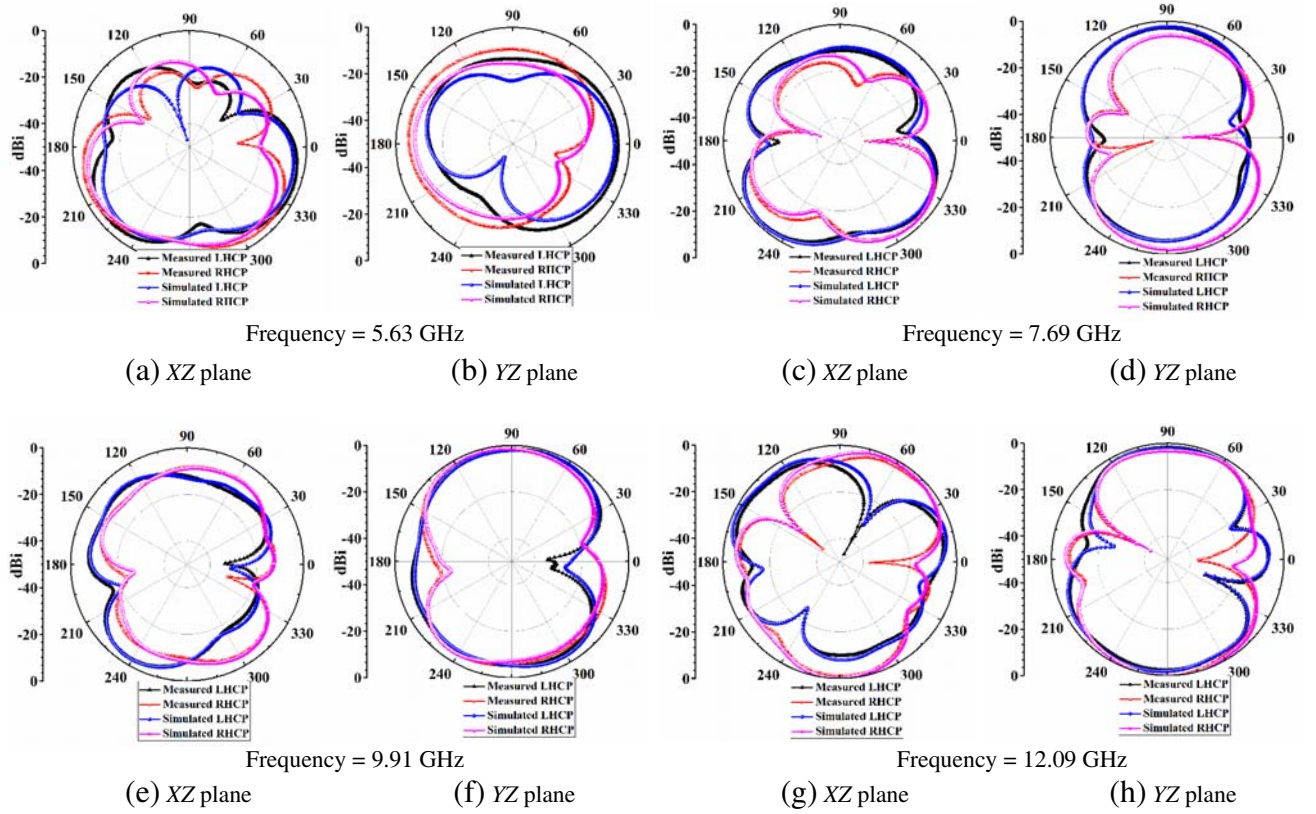
Frequency = 5.63 GHz   Frequency = 7.69 GHz

(a) *XZ* plane   (b) *YZ* plane   (c) *XZ* plane   (d) *YZ* plane

Frequency = 9.91 GHz   Frequency = 12.09 GHz

(e) *XZ* plane   (f) *YZ* plane   (g) *XZ* plane   (h) *YZ* plane

Figure 10. Simulated radiation patterns (LHCP and RHCP) in the (c), (e), (g) for XZ ($\varphi = 0°$) and (b), (d), (f), (h) for YZ ($\varphi = 90°$) planes.
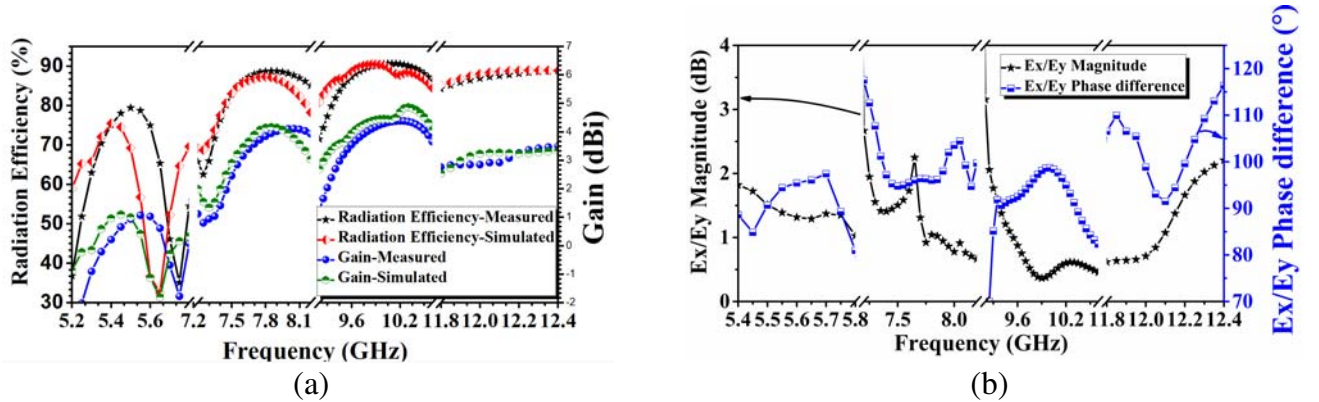

Figure 11. Implemented antenna: (a) measured, simulated gain and radiation efficiency plot vs. frequency; (b) simulated E_X/E_Y magnitude and phase plot vs. frequency.

5.2. Simulations of Antenna Parameters and Discussions

Figure 7(b) depicts the comparison of simulated ARBWs of the two prototypes (Antenna.5 and Antenna.6) of the monopole antenna. For the symmetric CPW-fed ground plane cases, due to strong standing wave along its width, the radiation is linearly polarized at 5.63 GHz, and the AR values are large at this frequency. With the introduction of CPW-fed asymmetric ground plane (from the feed gap left side area $L2 \times W2 = 0.062 \times 0.135\lambda_{gL}^2$ and right side area $L1 \times W1 = 0.091 \times 0.310\lambda_{gL}^2$), CP performance is achieved at $f_{cp1} = 5.63$ GHz. For the proposed case, a combination of two asymmetric

cross-shaped slits in centre position of the main radiator (areas $L3 \times W3 = 0.158 \times 0.038\lambda_{gL}^2$ and $L4 \times W4 = 0.192 \times 0.0096\lambda_{gL}^2$) leads to a new CP excitation at $f_{cp2} = 7.69$ GHz. Due to the presence of a rectangular open loop (length $L6 = 0.096\lambda_{gL}$, width $c1 = 0.156\lambda_{gL}$, thickness $d = 0.024\lambda_{gL}$, gap length $c3 = 0.036\lambda_{gL}$) at the right corner side of the radiator, another CP band is obtained at $f_{cp3} = 9.91$ GHz. The presence of the tuning stub (area $L5 \times W5 = 0.036 \times 0.36\lambda_{gL}^2$) in the feeding structure generates the fourth CP band at $f_{cp4} = 12.09$ GHz. In conclusion, the utilization of the proposed radiator has given not only multiple wide impedance bandwidths but also quad bands CP performance as shown in Figs. 12(a)–(d).

The simulated surface current distribution of the presented antenna at $f_{cp1} = 5.63$ GHz is shown in Fig. 13. The CP waves originate from the alternate excitation of the asymmetric CPW-fed ground and the annular stack patch with eight symmetrical slots along its periphery. The current components in vertical direction transpire along the slots of annular ring, and the horizontal current components originate from asymmetric CPW-fed ground. Fig. 14 presents the simulated electric current distributions of the implemented antenna at $f_{cp2} = 7.69$ GHz. The current components in vertical direction transpire along the two asymmetric cross shaped slits in centre position, and the horizontal current components originate from annular ring. Fig. 15 represents the simulated electric current distributions for the antenna at $f_{cp3} = 9.91$ GHz. The current components in vertical direction transpire along the rectangular open loop, and the horizontal current components originate from annular ring. Similarly, Fig. 16 represents the simulated electric current distributions for the antenna at $f_{cp3} = 12.09$ GHz. The current components in vertical direction transpire along the feed line, and the horizontal current components originate from the stub on the feeding element. So, these surface
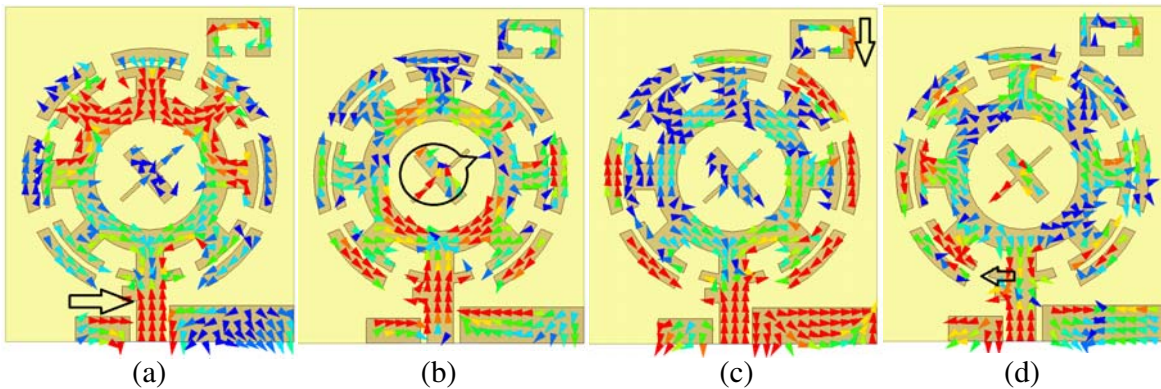

Figure 12. Simulated surface current distributions of the implemented antenna at CP resonating frequencies: (a) $f_{cp1} = 5.63$ GHz; (b) $f_{cp2} = 7.69$ GHz; (c) $f_{cp3} = 9.91$ GHz; (d) $f_{cp4} = 12.09$ GHz.
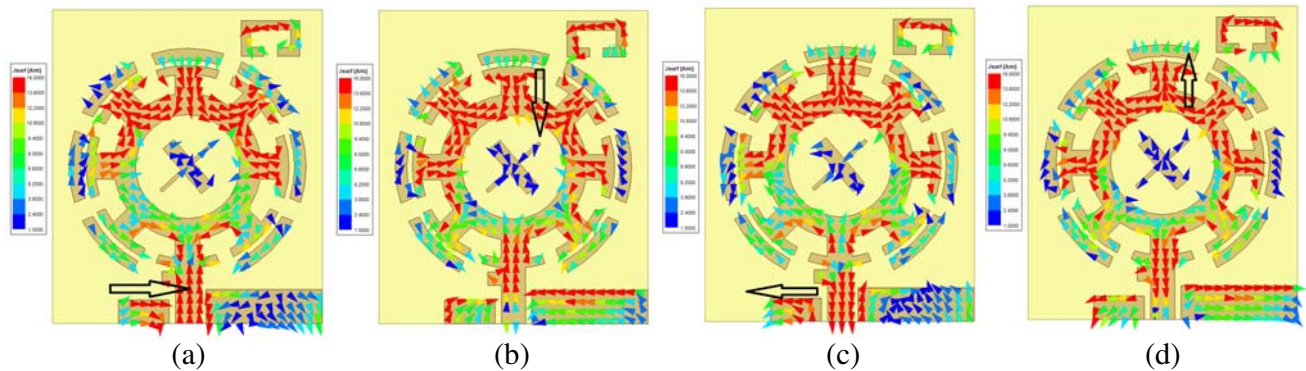

Figure 13. Distribution current on the surface (simulated) for phases of (a) 0°, (b) 90°, (c) 180° and (d) 270° at $f_{cp1} = 5.63$ GHz.
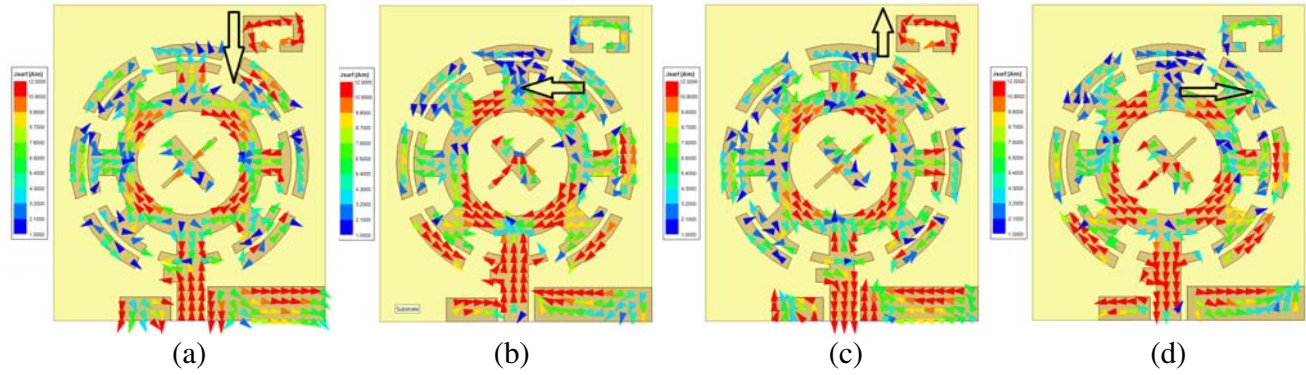
Figure 14. Distribution current on the surface (simulated) for phases of (a) 0°, (b) 90°, (c) 180° and (d) 270° at $f_{cp2} = 7.69$ GHz.
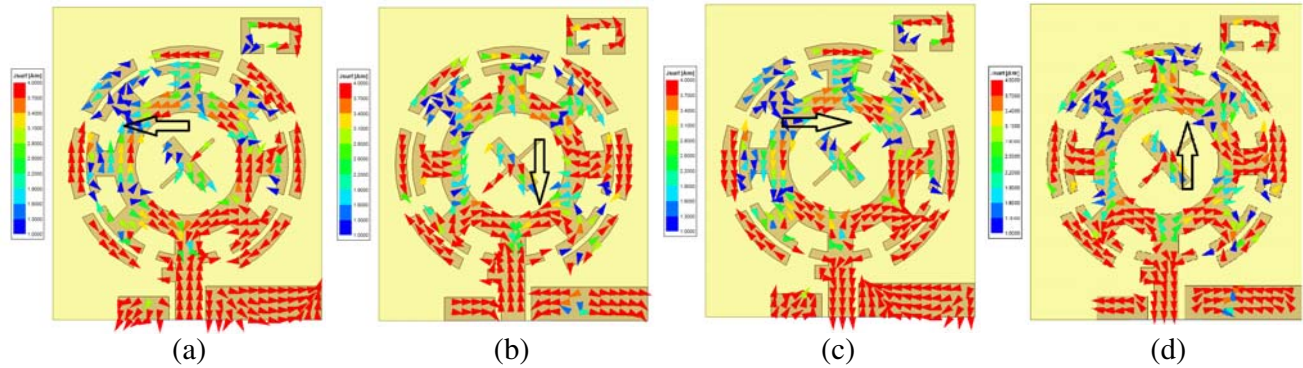

Figure 15. Distribution current on the surface (simulated) for phases of (a) 0°, (b) 90°, (c) 180° and (d) 270° at $f_{cp3} = 9.91$ GHz.

current distribution analyses in Figs. 13–16 deduce a quad-band CP performance at their respective CP resonating frequencies.

5.3. Effect of Length and Width of the CPW-Feed on IBW and ARBW

In the CM analysis, infinite ground plane is assumed, and the feeding network is not considered. In the actual design, an asymmetric CPW-fed ground plane is used. It is necessary to study the effect of the feeding parameters on the proposed antenna. In this section, the effects of only the crucial parameters $L1$ and $W2$ on the resulting reflection coefficient and axial ratio bandwidth are discussed. When a parameter is studied, dimensions of others remain unchanged.

Through extensive parametric studies, it has been established that the length of left CPW-fed ground plane ($L1$) and width of right CPW-fed ground plane ($W2$) contribute significantly in producing the return-loss curve. A program in MATLAB is written for interpolation and optimization of $L1$ and $W2$. Simulations for parametric analysis of $L1$, $W2$ over whole frequency band of these parameters of the CPW-fed ground are plotted in Fig. 17(a). It is noted that a local minimum is there in the impedance band curve and maximum IBW that occurs when $L1 = 3.8$ mm and $W2 = 5.65$ mm. Fig. 17(b) shows the simulated contour plot for the variation of $L1$ and $W2$ with respect to operating frequency region. Through similar exhaustive parametric studies, it was established that $L1$ and $W2$ play important roles in producing the ARBW (< 3 dB) curve. A program in Python has been written for interpolation, design of variation, and optimization of $L1$ and $W2$. It can be seen from this contour diagram that when the optimized value of $L1 = 3.8$ mm and $W2 = 5.65$ mm, the ARBW is maximum giving quad CP bands over this operating frequency.
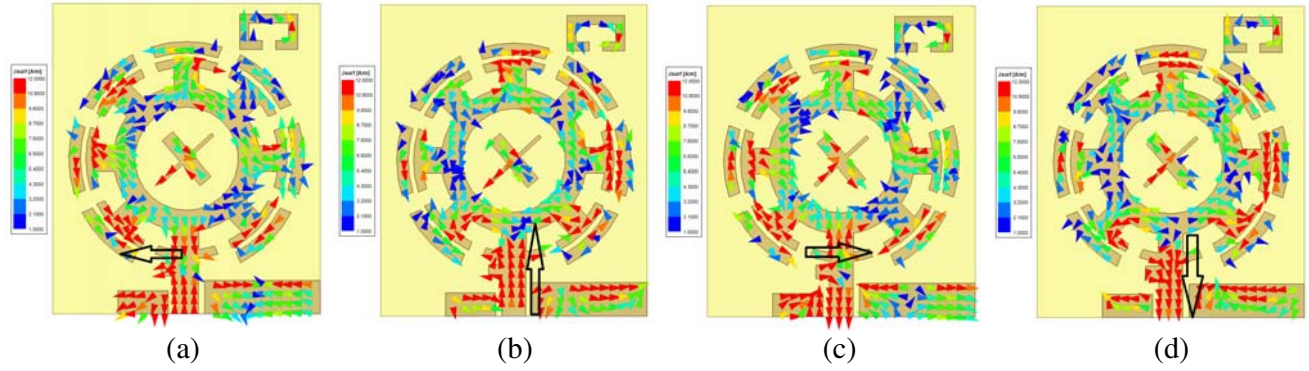
Figure 16. Distribution current on the surface (simulated) for phases of (a) 0°, (b) 90°, (c) 180° and (d) 270° at $f_{cp4} = 12.09$ GHz.
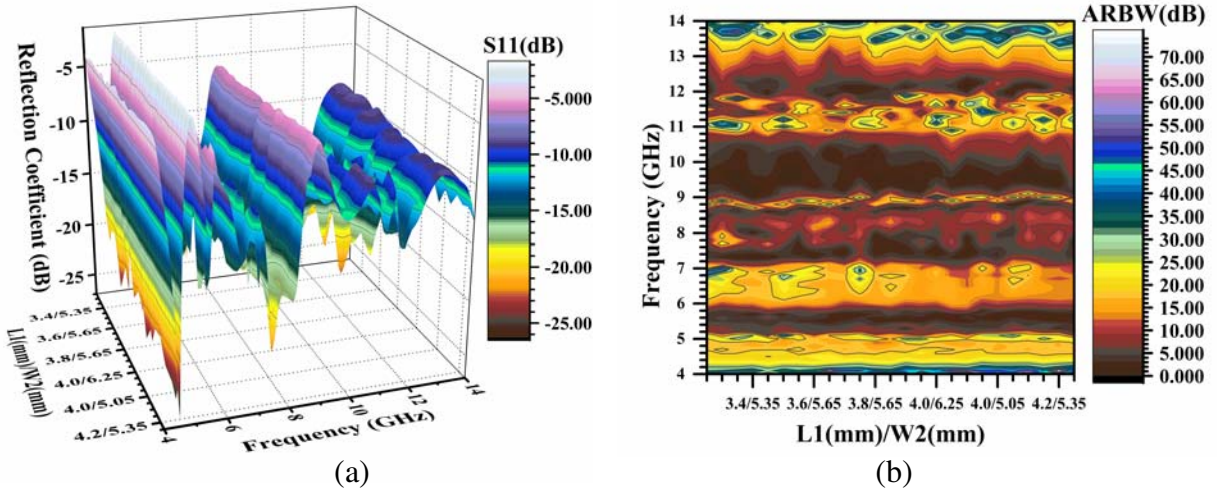

Figure 17. (a) Simulated reflection coefficient over frequency band for different parametric values of $L1$ (mm) and $W2$ (mm); (b) simulated contour plot of ARBW over the operating frequency band with changing of $L1$ (mm) and $W2$ (mm).

5.4. The Influence of the SMA Connector on IBW and ARBW

The influences of the SubMiniature version A (SMA) connector on IBW (Fig. 18(a)) and ARBW (Fig. 18(b)) were simulated and compared both with simulated results without SMA connector and actual measured results of fabricated antenna with the SMA. From Fig. 18(a) it can be said that reflection coefficient curves for the SMA connector simulated and measured results are well matched, but simulation results without SMA connector deviate a little in the higher frequency range. From Fig. 18(b) it can also be said that simulated (with SMA) ARBW bands match well with both measured (SMA) and simulated (without SMA) results. Some little differences are observed in higher frequency region with simulation (with SMA) which may be due to phase changes. The detailed dimensions and structure of the simulated model for the used SMA connector are shown in Fig. 18(c). The SMA connector is filled with Teflon to provide mechanical strength. Fig. 18(c) also shows the simulation model for this proposed antenna with SMA connector.

The influence of the SMA connector can be de-embedded or removed from the measured and simulated S_{11} by the following relation [35].

$$S_{11}^{\text{De-embedded SMA}} = S_{11}^{\text{SMA-W}} \times e^{(2j\beta h_s)} \tag{7}$$

where β = phase constant = $\omega\sqrt{\mu\varepsilon}$, and ω, μ, ε are the annular frequency, permittivity, permeability
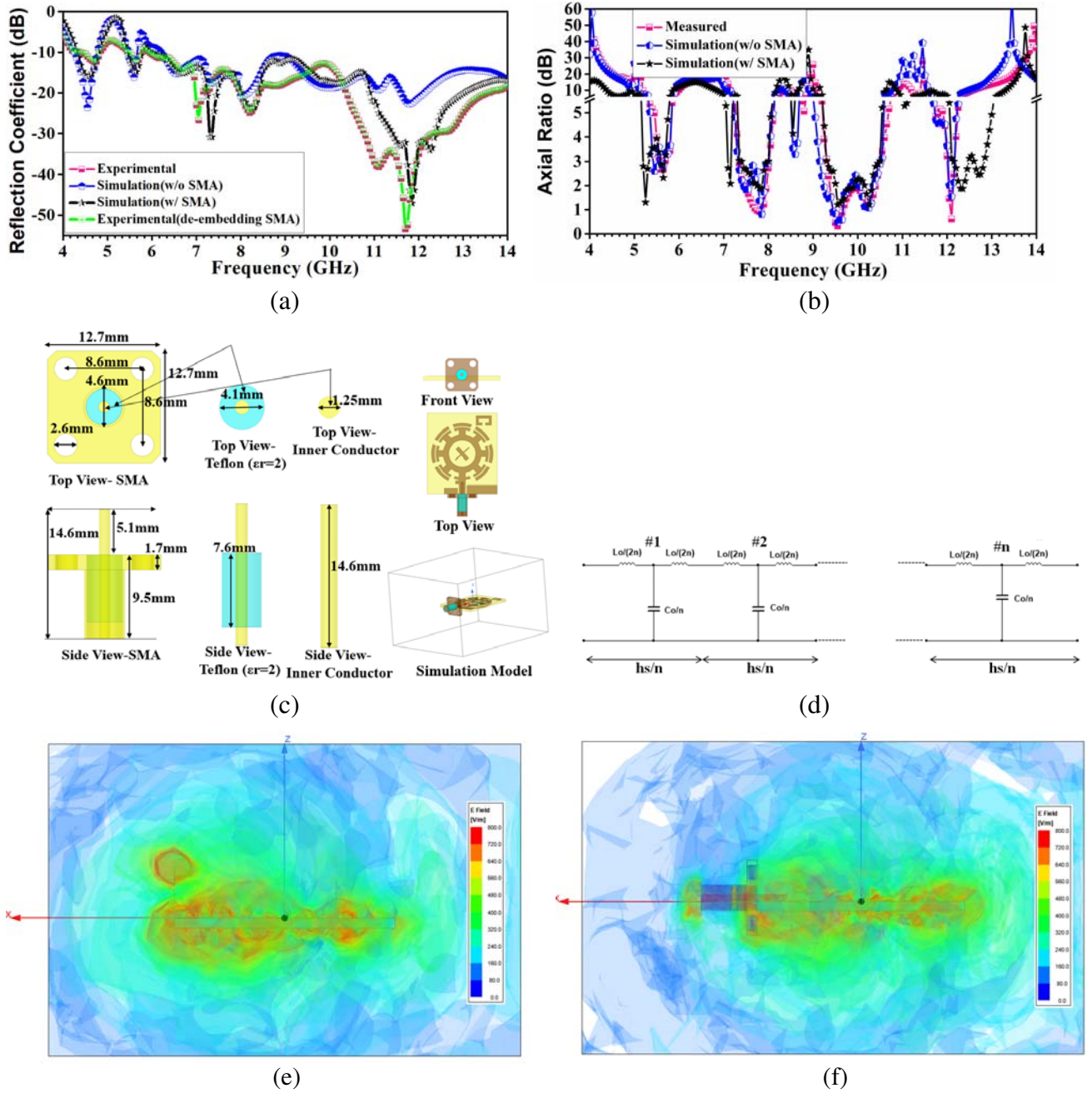
Figure 18. (a) Reflection coefficient vs. frequency characteristics; (b) ARBW vs. frequency characteristics; (c) simulation model of SMA connector for proposed antenna; (d) SMA connector equivalent LC ladder circuit model; (e) electric field intensity for the proposed antenna (without SMA) in XZ plane (10.5 GHz); (f) electric field intensity for the proposed antenna (SMA) in XZ plane (10.5 GHz).

of the SMA connector, correspondingly. Here, h_s is the height of the Teflon layer in SMA connector, and $S_{11}^{\text{SMA-W}}$ is the value of S_{11} with SMA connector. Additionally, the de-embedded measured result by using Equation (7) is shown in Fig. 18(a). This result is in good agreement with the simulation if the SMA connector is not taken into account.

In Fig. 18(c), a = inner conductor radius and b = outer radius of Teflon layer in SMA connector. L and C are the series inductance and parallel capacitance per unit length as shown in Fig. 18(d). L

and C are expressed as

$$C = \frac{2\pi\varepsilon_r\varepsilon_0}{\log\frac{b}{a}} \tag{8}$$

$$L = \frac{\mu_0}{2\pi}\log\frac{b}{a} \tag{9}$$

where ε_0 and μ_0 are the permittivity and permeability in free space. Then the characteristic impedance becomes

$$Z_c = \sqrt{\frac{L}{c}} = \sqrt{\frac{\mu_0}{\varepsilon_r\varepsilon_0}}\frac{\log\frac{b}{a}}{2\pi} \tag{10}$$

By replacing the parameters in Equation (10) by the values given in Fig. 18(c), obtain $Z_c = 50.4\,\Omega$ for the SMA connector, which is well matched with antenna characteristics impedance ($50\,\Omega$).

Figures 18(e)–(f) show the distribution of electric field intensity in the xz plane for simulation modelling of antenna without SMA and with SMA connector, respectively. For the case of '(e)' a $50\,\Omega$ lumped port excitation is used, whereas for the case '(f)' the outer conductor and holder of SMA connector, the electromagnetic fields affect them. This is due to the impinging effect of the electromagnetic wave on the outer conductor and holder of SMA connector which is radiated from proposed antenna. Therefore, the simulation results of IBW and ARBW without SMA connector vary little, particularly in the higher frequency region, with that of simulated and measured results with SMA connector.

5.5. Comparison of the Proposed Antenna with Related Designs

In Table 1, comparison is drawn between the proposed antenna and some very recently designed quad band CP antennas. It transpires that the proposed antenna shows the widest IBW with quad CP characteristics, stable radiation patterns, and fair peak gain. It is also compact in size.

Table 1. Comparison with related quad-band CP antennas.

Ref. (Year)	Antenna Size — λ_{gL}^3 (mm³), Substrate material	IBW-GHz (%)	ARBW-GHz (%)
10 (2015)	Not Mentioned, RO3003	4.97–6.49 (26.53)	5.122–5.173 (0.99), 5.471–5.71 (4.27), 6.275–6.331 (0.89), 7.677–7.782 (1.36)
11 (2015)	0.674 × 0.713 × 0.02 (52 × 55 × 1.52), Taconic RF-5	2.37–2.75 (14.84), 3.4–8 (80.7)	2.35–2.48 (5.58), 3.45–3.75 (8.33), 5.25–5.45 (3.74), 5.7–5.87 (2.94)
12 (2018)	0.42 × 0.499 × 0.021 (32 × 38 × 1.6), FR4-epoxy	2.4–2.6 (8.8), 2.9–3.1 (6.67), 3.3–3.5 (5.8), 4–8.3 (69.92)	2.39–2.55 (6.48), 3.05–3.1 (1.63), 4–5 (22.22), 6.3–6.64 (5.25)
13 (2019)	0.955 × 0.828 × 0.021 (75 × 65 × 1.62), Taconic TLY-5	2.33–5.70 (83.93)	2.38–2.56 (4.92), 2.75–3.03 (9.69), 3.42–3.53 (3.16), 5.16–5.54 (7.1)
Proposed Work	0.84 × 0.725 × 0.038 (35 × 30 × 1.6), FR4-epoxy	4.36–4.82 (10.02), 5.5–5.78 (4.96), 5.95–beyond 14 GHz (> 80.7)	5.57–5.69 (2.13), 7.36–8.01 (8.46), 9.31–10.51 (12.11), 12.01–12.17 (1.32)

6. CONCLUSION

A three-step design procedure using TCM has been utilized to design a quad band monopole antenna consisting of a novel annular ring radiator. It has been revealed that the structure can support three dominant modes over the frequency band of interest. CMA helped in locating these dominant modes, radiation parameters and position of feed line. Asymmetric CPW-fed ground has been used to selectively excite the three desired modes with symmetric currents and an additional CP resonance at 5.63 GHz. Tuning of the length and width of the asymmetric CPW-fed ground plane plays a crucial role in achieving wide impedance band. The measured IBW ranges in 4.36–4.82 GHz, 5.50–5.78 GHz, and 5.95–beyond 14 GHz. The measured quad CP bands obtained inside the IBW curves and range in 5.57–5.69 GHz, 7.36–8.01 GHz, 9.31–10.51 GHz, and 12.01–12.17 GHz. All measured data faithfully validate simulation results. Measured results confirm that the proposed antenna exhibits high gain and can be used for C band (4–8 GHz), X band (8–12 GHz) and 5 GHz WLAN, FIXED Satellite, radiolocation application devices. The proposed design is compact, efficient and furnishes wider quad CP bands than recently reported related quad-band CP antennas.

ACKNOWLEDGMENT

REFERENCES

1. Toh, B. Y., R. Cahill, and V. F. Fusco, "Understanding and measuring circular polarization," *IEEE Transactions on Education*, Vol. 46, No. 3, 313–318, 2003, doi: 10.1109/TE.2003.813519.

2. Gao, S., Q. Luo, and F. Zhu, *Circularly Polarized Antennas*, John Wiley & Sons, Chichester, UK, 2013.

3. Kumar, G. and K. P. Ray, *Broadband Microstrip Antennas*, Artech House, Boston, MA and London, UK, 2003.

4. Kurniawan, F., J. T. Sri Sumantyo, K. Ito, H. Kuze, and S. Gao, "Patch antenna using rectangular centre slot and circular ground slot for Circularly Polarized Synthetic Aperture Radar (CP-SAR) application," *Progress In Electromagnetics Research*, Vol. 160, 51–61, 2017.

5. Mekimah, B., T. Djerafi, A. Messai, and A. Belhedri, "Broadband circularly polarized CPW-fed asymmetrically-shaped slot patch antenna for X band applications," *Progress In Electromagnetics Research Letters*, Vol. 91, 137–143, 2020.

6. Yuan, J. and Y. Li, "A compact circularly polarized microstrip ring antenna using a slotted ground for GNSS applications," *Progress In Electromagnetics Research Letters*, Vol. 88, 29–36, 2020.

7. Wu, Z., G. M. Wei, X. Li, and L. Yang, "A single-layer and compact circularly polarized wideband slot antenna based on "bent feed"," *Progress In Electromagnetics Research Letters*, Vol. 72, 39–44, 2018.

8. Birwal, A., S. Singh, B. K. Kanaujia, and S. Kumar, "CPW-fed ultra-wideband dual-sense circularly polarized slot antenna," *Progress In Electromagnetics Research C*, Vol. 94, 219–231, 2019.

9. Dhara, R. and M. Mitra, "A triple-band circularly polarized annular ring antenna with asymmetric ground plane for wireless applications," *Engineering Reports*, Vol. 2, No. 4, e12150, 2020, doi: 10.1002/eng2.12150.

10. Singh, D. K., B. K. Kanaujia, S. Dwari, G. P. Pandey, and S. Kumar, "Novel quad-band circularly polarized capacitive-fed microstrip antenna for C-band applications," *Microwave and Optical Technology Letters*, Vol. 57, No. 11, 2622–2628, 2015, doi: 10.1002/mop.

11. Hoang, T. V., T. T. Le, Q. Y. Li, and H. C. Park, "Quad-band circularly polarized antenna for 2.4/5.3/5.8-GHz WLAN and 3.5-GHz WiMAX applications," *IEEE Antennas and Wireless Propagation Letters*, Vol. 15, 1032–1035, 2015, doi: 10.1109/LAWP.2015.2490258.

12. Rao, M. V., B. T. P. Madhav, T. Anilkumar, and B. P. Nadh, "Metamaterial inspired quad band circularly polarized antenna for WLAN/ISM/Bluetooth/WiMAX and satellite communication applications," *AEU-International Journal of Electronics and Communications*, Vol. 97, 229–241, 2018, doi: 10.1016/j.aeue.2018.10.018.

13. Le, T. T. and T. Y. Yun, "A quad-band dual-sense circularly-polarized square-ring antenna for multi-functional wireless applications," *IEEE Access*, Vol. 7, 149634–149640, 2019, doi: 10.1109/ACCESS.2019.2947094.

14. Garbacz, R. and R. Turpin, "A generalized expansion for radiated and scattered fields," *IEEE Transactions on Antennas and Propagation*, Vol. 19, No. 3, 348–358, 1971, doi: 10.1109/TAP.1971.1139935.

15. Harrington, R. and J. Mautz, "Theory of characteristic modes for conducting bodies," *IEEE Transactions on Antennas and Propagation*, Vol. 19, No. 5, 622–628, 1971, doi: 10.1109/TAP.1971.1139999.

16. Harrington, R. and J. Mautz, "Computation of characteristic modes for conducting bodies," *IEEE Transactions on Antennas and Propagation*, Vol. 19, No. 5, 629–639, 1971, doi: 10.1109/TAP.1971.1139990.

17. Chen, Y. and C. F. Wang, *Characteristic Modes: Theory and Applications in Antenna Engineering*, John Wiley & Sons, Hoboken, New Jersey, USA, 2015.

18. Zhao, C. and C. F. Wang, "Characteristic mode design of wide band circularly polarized patch antenna consisting of H-shaped unit cells," *IEEE Access*, Vol. 6, 25292–25299, 2018, doi: 10.1109/ACCESS.2018.2828878.

19. Wen, D., Y. Hao, H. Wang, and H. Zhou, "Design of a wideband antenna with stable omnidirectional radiation pattern using the theory of characteristic modes," *IEEE Transactions on Antennas and Propagation*, Vol. 65, No. 5, 2671–2676, 2017, doi: 10.1109/TAP.2017.2679767.

20. Wang, C., Y. Chen, and S. Yang, "Bandwidth enhancement of a dual-polarized slot antenna using characteristic modes," *IEEE Antennas and Wireless Propagation Letters*, Vol. 17, No. 6, 988–992, 2018, doi: 10.1109/LAWP.2018.2828881.

21. Saraswat, K. and A. R. Harish, "Analysis of wideband circularly polarized ring slot antenna using characteristics mode for bandwidth enhancement," *International Journal of RF and Microwave Computer-Aided Engineering*, Vol. 28, No. 2, e21186, 2018, doi: 10.1002/mmce.21186.

22. Li, K. and Y. Shi, "Wideband MIMO handset antenna design based on theory of characteristic modes," *International Journal of RF and Microwave Computer-Aided Engineering*, Vol. 28, No. 4, e21217, 2018, doi: 10.1002/mmce.21217.

23. Ghalib, A. and M. S. Sharawi, "New antenna mode generation based on theory of characteristic modes," *International Journal of RF and Microwave Computer-Aided Engineering*, Vol. 29, No. 6, e21686, 2019, doi: 10.1002/mmce.21686.

24. Kumar, N. and R. Khanna, "A compact multi-band multi-input multi-output antenna for 4G/5G and IoT devices using theory of characteristic modes," *International Journal of RF and Microwave Computer-Aided Engineering*, Vol. 30, No. 1, e22012, 2020, doi: 10.1002/mmce.22012.

25. Jaiverdhan, M. M. Sharma, R. P. Yadav, and R. Dhara, "Characteristic mode analysis and design of broadband circularly polarized CPW-fed compact printed square slot antenna," *Progress In Electromagnetics Research M*, Vol. 94, 105–118, 2020.

26. Kurniawan, F., J. T. Sri Sumantyo, K. Ito, H. Kuze, and S. Gao, "Patch antenna using rectangular centre slot and circular ground slot for Circularly Polarized Synthetic Aperture Radar (CP-SAR) application," *Progress In Electromagnetics Research*, Vol. 160, 51–61, 2017.

27. Dhara, R. and T. Kundu, "A compact inverted Y-shaped circularly polarized wideband monopole antenna with open loop," *Engineering Reports*, Vol. 2, No. 11, eng2.12326, 2020, doi: 10.1002/eng2.12326.

28. Felegari, N., J. Nourinia, C. Ghobadi, and J. Pourahmadazar, "Broadband CPW-fed circularly polarized square slot antenna with three inverted-L-shape grounded strips," *IEEE Antennas and Wireless Propagation Letters*, Vol. 10, 274–277, 2011, doi: 10.1109/LAWP.2011.2135832.

29. Gupta, A., B. Bansal, V. K. Mishra, and A. Agrawal, "Miniaturised tri-band rhombus-shaped metamaterial-inspired antenna with gain enhancement using complementary closed ring resonators," *IET Microwaves, Antennas and Propagation*, Vol. 14, No. 2, 185–193, 2019, doi: 10.1049/iet-map.2019.0567.

30. Lin, F. H. and Z. N. Chen, "Low-profile wideband metasurface antennas using characteristic mode analysis," *IEEE Transactions on Antennas and Propagation*, Vol. 65, No. 4, 1706–1713, 2017, doi: 10.1109/TAP.2017.2671036.

31. Lin, F. H. and Z. N. Chen, "A method of suppressing higher order modes for improving radiation performance of metasurface multiport antennas using characteristic mode analysis," *IEEE Transactions on Antennas and Propagation*, Vol. 66, No. 4, 1894–1902, 2018, doi: 10.1109/TAP.2018.2806401.

32. Lin, F. H. and Z. N. Chen, "Truncated impedance sheet model for low-profile broadband nonresonant-cell metasurface antennas using characteristic mode analysis," *IEEE Transactions on Antennas and Propagation*, Vol. 66, No. 10, 5043–5051, 2018, doi: 10.1109/TAP.2018.2854366.

33. Dhara, R., "Quad-band circularly polarized CPW-fed G-shaped printed antenna with square slot," *Radioelectronics and Communications Systems*, Vol. 63, No. 7, 376–385, 2020, doi: 10.3103/S0735272720070055.

34. Dhara, R., S. K. Jana, and M. Mitra, "Tri-band circularly polarized monopole antenna for wireless communication application," *Radioelectronics and Communications Systems*, Vol. 63, No. 4, 213–222, 2020, doi: 10.3103/S0735272720040044.

35. Hirano, T., J. Hirokawa, and M. Ando, "Influence of the SMA connector and its modeling on electromagnetic simulation," *Microwave and Optical Technology Letters*, Vol. 57, No. 9, 2168–2171, 2015, doi: 10.1002/mop.29304.